Silver centers luminescence in phosphate glasses subjected to X-Rays or combined X-rays and femtosecond laser exposure

Théo Guérineau, Francesca Cova, Yannick Petit, Alain Abou Khalil, Alexandre Fargues, Marc Dussauze, Sylvain Danto, Anna Vedda, Lionel Canioni, Thierry Cardinal

Silver centers luminescence in phosphate glasses subjected to X-Rays or combined X-rays and femtosecond laser exposure

Théo GUERINEAU,[1] Francesca COVA,[2] Yannick PETIT,[1,3] Alain ABOU KHALIL,[3] Alexandre FARGUES,[1] Marc DUSSAUZE,[4] Sylvain DANTO,[1] Anna VEDDA,[2] Lionel CANIONI[3] and Thierry CARDINAL[1]

[1] *Université de Bordeaux, CNRS, ICMCB, UPR 9048, F-33608 Pessac, France*

[2] *Department of Materials Science, University of Milano-Bicocca, 20125 Milan, Italy*

[3] *Université de Bordeaux, CNRS, CEA, CELIA, UMR 5107, F-33405 Talence, France*

[4] *Université de Bordeaux, ISM, CNRS, UMR 5255, F-33405 Talence, France*

Abstract

The generation of silver species has been investigated in silver containing sodo-gallo-phosphate glasses subjected to X-rays irradiations. Radio-luminescence spectroscopy has evidenced the presence of isolated and paired silver ions. The proportion of silver pairing is found dominant in ortho-phosphate glass compositions, compared to poly-phosphate counterparts. The phosphate glass network is reported to have a decisive impact on the X-Ray photosensitivity and the formation of luminescent silver species, namely Ag^{2+} hole trap silver ions and Ag_m^{x+} silver clusters. The subsistence of femtosecond laser produced silver luminescent structures under X-Ray irradiation has been demonstrated.

I. Introduction

Radio-Photo-Luminescence (RPL) of silver-containing phosphate glasses has been studied extensively since Schulman *et al* (1). Nowadays it is considered as a reliable radiation dosimetry technique (2). Extensively described in the literature (3–7), the RPL mechanism in silver-doped glass

remains a hot topic as no clear unanimity has been established concerning the nature of the centers responsible for the luminescence properties. During the irradiation process using ionizing radiations such as X-Ray or gamma radiations, exciton pairs are released in the glass matrix and then are proposed to recombine with the Ag^+ silver ions, leading to the formation of electron and hole trapped silver species, such as Ag^0 and Ag^{2+} respectively (8). Subsequently to this phenomenon, clustering process (9) may occur, then generating various silver clusters with a variety of charge and parity (10).

Recently, Direct Laser Writing (DLW) technique has offered new opportunities in silver containing glass modifications for fabricating integrated devices. Indeed, supported by the Ag^+ silver ions (11), the Infra-red femtosecond (IR fs) DLW enables the generation of local properties such as fluorescence (12–14), second (15,16) and third (17) order nonlinearities, plasmonic resonance (18,19) or localized refractive index change (20,21). Unlike current commercialized RPL dosimeters, a silver ion content by two-orders-of-magnitude higher is preferable for IR fs DLW. To our knowledge, no investigation combining RPL and IR fs DLW has been conducted on such glasses. Depending on the [O]/[P] Oxygen-to-Phosphorus ratio, the phosphate chain length can be described as a sequence of phosphorus tetrahedron of four different kinds. To define them, the phosphate tetrahedron is expresses as a Q^n units (22,23), where n denotes the number of bridging oxygen between phosphorus elements and Q the PO_4 tetrahedron. The poly-phosphate glass exhibits long chains of Q^2 entities while pyro- and ortho-phosphate exhibit a majority of Q^1 paired and Q^0 isolated PO_4 tetrahedra, respectively. Commonly conducted in silver-containing pyro-phosphate glasses, IR fs DLW has been also carried out on both poly- and ortho-phosphate compositions in the system Na_2O-P_2O_5-Ga_2O_3 to evaluate the glass network influence on IR fs laser photosensitivity (12). We show that ortho-phosphate and pyro-phosphate glass networks exhibit higher photosensitivity for fs DLW as compared to the poly-phosphate glass.

In this paper, we report the impacts of X-rays irradiation of silver-containing ortho- and pyro-phosphates in the glass system Na_2O-P_2O_5-Ga_2O_3 (labelled as GPN_o and GPN_p glasses, respectively) in term of photosensitivity and generation of luminescent silver centers. Absorption, steady state and

time resolved luminescence spectroscopies have been conducted. Moreover, the impact of X-Rays irradiation on IR fs DLW structures using micro-luminescence spectroscopy has been investigated.

II. Experimental procedures

II-1. Glass preparation

From the ternary diagram P_2O_5-Ga_2O_3-Na_2O, selected pyro and ortho-phosphate glass compositions have been elaborated and doped with a fixed amount of silver oxide (2 mol%). Both glasses were synthesized from H_3PO_4 (Roth, 85%), Na_2CO_3 (Alfa Aesar, 99.95%), Ga_2O_3 (Strem Chemicals, 99.998%) and $AgNO_3$ (Alfa Aesar, 99.995%) precursors. These precursors are all mixed into a Teflon beaker in aqueous solution and dried on a sand bath during 12 hours. After a grind step, the obtained powder was melted at 1050 °C and 1400 °C, respectively for the pyro and ortho-phosphate, for 24 hours to optimize the Ag^+ silver ions homogenization. To reduce the mechanical constraints, glasses were annealed 30 °C below the glass transition temperature (T_g) for 4 hours, then cut and optically polished on both parallel faces.

II-2. Infrared femtosecond Direct Laser Writing (DLW)

Infrared (IR) femtosecond (fs) DLW were carried out with a KGW:Yb femtosecond oscillator (up to 2.6 W, 10 MHz and 390 fs FWHM at 1030 nm) combined with an acousto-optic modulator in order to control the energy and number of pulses. The DLW structures were generated using a Zeiss microscope objective (20x, 0.75 NA), focusing 160 µm below the glass surface. In order to eliminate spherical aberrations, a spatial light modulator (LCOS; X10468-03, Hamamatsu Photonics) was used. The sample positioning and displacements were performed with a 3D translation stage XMS-50, enabling a precision up to 50 nm.

II-3. Radio-luminescence, radio-photo-luminescence and X-Rays irradiation

Radio-luminescence (RL) and radio-photo-luminescence (RPL) measurements were conducted using a homemade apparatus at the Department of Materials Science of the University of Milano-

Bicocca. The setup consists of back-illuminated, UV-enhanced, liquid nitrogen-cooled CCD detector (Jobin-Yvon Spectrum One 3000) coupled to a monochromator (Jobin-Yvon Triax 180). The RL experiment consists in monitoring the emitted light during a continuous irradiation of a sample with X-rays. For RL and RPL irradiations, a Philips PW2274 X-rays tube with tungsten anode (operating at respectively 20 or 32 kV) was used. At these voltages, the bremsstrahlung process drives the X-rays generation mechanism. The excitation laser diode was an export mod. LCS-DTL-374QT 355 nm operating with the 3rd harmonic of a Nd:YAG laser (pulse width of 5 ns, repetition rate of 20 KHz and 5 mW power). A circular Al mask with a diameter of 5 mm limits the irradiated area allowing for a quantitative comparison between samples (RL and RPL) and the localization of the X-rays irradiation and laser probed area (mainly useful for the localized DLW induced structures during the RPL). The dose values reported in the article for X-rays irradiations were obtained by comparison with a calibrated ^{90}Sr - ^{90}Y beta radioactive source and using optically stimulated luminescence emission from quartz crystalline powder (100 - 200 µm). For the X-rays induced optical absorption study, the samples were irradiated with a Machlett OEG50 X-ray tube with tungsten anode, operating at 32 kV. Also in this case, X-rays are produced by bremsstrahlung. Dose evaluation was performed by a PTW Duplex calibrated ionization chamber.

II-4. Pristine glass characterization

Micro-Raman spectroscopy was conducted on both compositions at room temperature thanks to a LABRAM 800-HR Raman spectrometer (Horiba Jobin-Yvon) with a single longitudinal mode laser source at 532 nm, coupled with a microscope objective (50×, NA 0.75) assuring the micron-scale spatial resolution. All spectra were recorded from 600 to 1400 cm^{-1} with a 2.5 cm^{-1} resolution.

UV-Visible transmission spectra were recorded with a Cary 5000 (Varian) spectrometer in the range 200 – 800 nm with a step of 1 nm and an integration time of 0.1 s.

The refractive indices were measured at 589 nm with an Abbe refractometer enabling a precision of ± 0.002.

A Fisher scientific Sartorius YDK01 was used to performed the density determination by Archimedes' method at room temperature and by immerging the glasses in diethyl phthalate.

The glass transition temperature was determined by measuring the differential scanning calorimetry on a Netzsch DTA 404 PC apparatus in DSC mode, on glass chunks in a Pt pan up to 650 °C at a heating rate of 10 °C.min^{-1} and a precision of ±3 °C.

II-5. Post DLW/X-Rays irradiated glass characterization

The micro-luminescence was carried out with a LABRAM 800-HR spectrophotometer (Horiba Jobin-Yvon) equipped with an Olympus microscope objective (100×, NA 0.9), a CW laser diode excitation at 405 nm (100 mW, TEM00, OBIS, COHERENT) and a thermoelectric cooled CCD camera (Synapse Model 354308). A correction function determined by two reference samples with broad spectral emission was used to correct the recorded spectra.

The UV-Visible transmission spectra were recorded with the same apparatus as that for the pristine glasses, in the same conditions. Note that the absorption spectra have been also collected over the entire glass thickness after DLW and/or X-rays irradiations.

The excitation spectra were recorded with a SPEX Fluorolog-2 spectrofluorimeter (Horiba Jobin-Yvon) at room temperature, equipped with a 450 W xenon lamp and a Hamamatsu R298 photomultiplier. The emission spectra were recorded at room temperature with an Edinburgh Analytical Instruments M300 Monochromator, a Xe-900 lamp and an AMHERST SCIENTIFIC CORP. 4100 cooled PMT.

The lifetime results have been extracted from time-resolved spectroscopy. A Continuum Surelite SL II-10 laser was used as a pulsed 355 nm excitation source (10 Hz, 70 mJ, 4-6 ns) followed by a half wave plate and a polarized beam splitter in order to control the laser pulse fluence, ensuring that the measurement behaves only as an excitation regime in a lifetime probing regime (and not in an irradiance regime that would lead to a glass modifications). Emission spectra were recorded thanks to a monochromator and a gated ICCD camera (Andor) being optically trigged by the pulsed UV laser.

III. Results

III-1. Structural impact on X-Rays irradiated phosphate photosensitivity

The pristine glass properties of both selected silver-doped phosphate glasses have been measured. Hereafter in Table 1 is reported their nominal glass composition, O/P ratio, density, refractive index, and glass transition temperature.

Table 1 Glass compositions and various properties of the considered GPN_p and GPN_o glasses

Acronym	Nominal cationic composition (%)				O/P ratio	Density (±0.005 g.cm^{-3})	n_{589} (±0.005)	T_g (±3 °C)
	$PO_{5/2}$	$GaO_{3/2}$	$NaO_{1/2}$	$AgO_{1/2}$				
GPN_p	56.0	28.0	14.0	2.0	3.4	3.15	1.566	497
GPN_o	31.0	20.6	46.4	2.0	4.3	3.08	1.541	385

Considering the nominal cationic compositions, one observes that for a constant silver amount the element percentages of the other compounds are shifting. The most important point lies in the atomic ratios O/P, which is equal to 3.4 for the GPN_p glass, typical of a pyro-phosphate (22), while it is 4.3 for the GPN_o, typical of an ortho-phosphate network (23) accordingly with Brow *et al.* nomenclature (22,23).

From a previous study (12), the glass network structure has been identified as a key point to explain the variation in the silver-doped phosphate glass photosensitivity, while silver content was kept the same. Hence, the Raman spectroscopy has been performed on the selected GPN_p and GPN_o glasses (Figure 1).

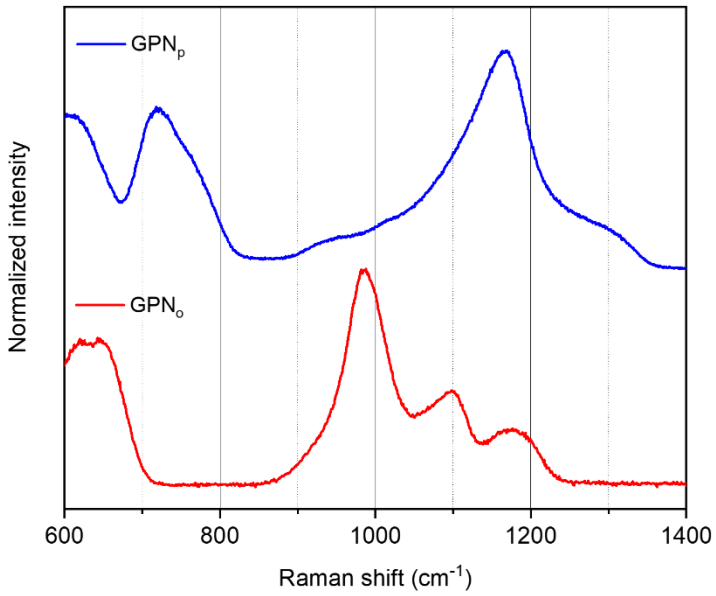

Figure 1 Normalized raw Raman spectra of GPN$_p$ and GPN$_o$ glasses

The Raman signature of GPN$_p$ (blue line) and GPN$_o$ (red line) glasses are presented in Figure 1. The GPN$_p$ sample features major contribution bands centered at 710 cm^{-1}, 740 cm^{-1} and 1160 cm^{-1}. The low frequency bands are assigned respectively to symmetric P-O-P bond stretching mode between two Q^2 phosphate tetrahedrons (22,24,25) and inside a phosphate tetrahedron dimeric entity (22,24–27), while the high frequency band is related to (PO_2^-) symmetric stretching vibrations in Q^2 (22,24,26,28). These considerations are consistent with a majority of Q^2 and Q^1 phosphate entities. Meanwhile, the GPN$_o$ glass exhibits low band intensities related to asymmetric (PO_3^{2-}) vibrations of Q^1 entities (24,26,28) as well as symmetric and asymmetric stretching of the Q^2 phosphate tetrahedron (22,24,26,28) respectively peaking at 1100 cm^{-1}, 1170 cm^{-1} and 1200 cm^{-1}. While the main contributions at 640 cm^{-1} and 980 cm^{-1}, respectively assigned to $[GaO_4]^-$ stretching vibrations (24–26,29–31) and symmetric (PO_4^{3-}) stretching in Q^0 phosphate entity (22,24) emphasizes a majority of Q^0 phosphate entities surrounded by sodium ions or gallium in tetrahedral sites $[GaO_4]^-$.

The radioluminescence measurements (RL) on the GPN$_p$ and GPN$_o$ glasses have been performed at a fixed dose rate while recording the emission spectra every 30 seconds, i.e. for subsequent cumulative doses. The RL spectra corresponding to an X-rays dose of 10 Gy are presented in Figure 2A for both glasses. During RL experiments, the X-rays photons are absorbed by the glass

phosphate network leading to radiative emissions specific of the Ag^+ silver ions. One emission band is observed with two contributions centered at 290 nm and 380 nm for the GPN_p glass (Figure 2A – blue curve) and only one at 380 nm for the GPN_o glass (Figure 2A – red curve). The emission at 290 nm is attributed to isolated Ag^+ silver ions and more precisely to the dipolar electric transition $4d^{10} \rightarrow 4d^9 5s^1$. When two Ag^+ silver ions are close enough, their atomic orbitals are slightly modified leading to the observable emission at 380 nm, such as the silver dimer Ag^+-Ag^+ observed in crystalline compounds under UV excitation (32). An experimental artefact at about 350 nm is present with a low emission intensity, which distorts the spectral distribution homothetically with the XR dose increase. The inset depicts the RL spectra from 10 to 625 Gy, normalized for the GPN_p glass. As the spectral shape remains perfectly constant for both glasses, the relative intensity has been integrated over the entire spectrum for the GPN_p sample, and from 275 to 600 nm for the GPN_o, and then normalized to the first integrated spectrum intensity. The resulting intensity evolution versus the X-rays dose is presented in Figure 2B. Both glasses present an intensity decrease by dose increasing, which is more pronounced for the ortho-phosphate glass.

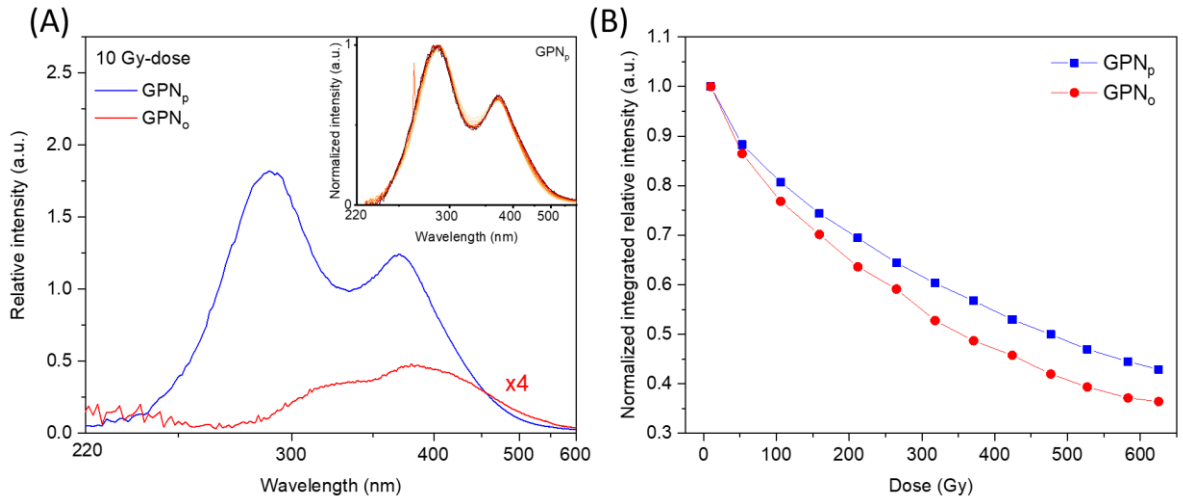

Figure 2 (A) Radioluminescence spectra for both GPN_p (blue curve) and GPN_o (red curve) glasses (inset: normalized GPN_p RL spectra from 10 to 625 Gy-doses. Note that the higher X-rays doses lead to the weaker normalized emission, as detailed hereafter in Figure 2B). (B) Evolution of the normalized integrated intensity versus dose for the GPN_p and GPN_o samples

The effective linear absorption coefficient (α) of both glasses is depicted in Figure 3A (GPN_p) and Figure 3B (GPN_o) after an X-rays irradiation series from 5 mGy to 3 kGy. The GPN_p and GPN_o pristine glasses do not present absorption above 300 nm. While increasing the X-rays dose, new absorption band contributions appear and grow with a maximum at about 320 nm for GPN_p and 360 nm for GPN_o, respectively. To better identify and track changes in the band contributions, the absorption coefficient difference spectra between 5 mGy dose versus unirradiated samples, 50 Gy versus 5 Gy dose, and 500 Gy versus 50 Gy dose samples for both studied GPN glasses have been performed as depicted in Figure 3C and Figure 3D. For the 5 mGy *vs.* Pristine difference spectrum of the GPN_p glass, a shoulder below 260 nm is revealed. This shoulder increases at higher X-rays doses such as in the 50 Gy *vs.* 5 Gy dose difference spectrum with complementary contribution bands at 320 and 390 nm.

Both absorption bands grow for 500 Gy *vs.* 50 Gy dose difference spectrum with an additional 290 nm-contribution band. For the GPN_o glass, the absorption contributions evolve differently. First, for the 5 mGy *vs.* Pristine dose difference spectrum, one band shoulder is observed below 300 nm. By increasing X-rays irradiation, the 50 Gy *vs.* 5 Gy dose difference spectrum highlights two main contributions at 320 and 350 nm, determined from a Gaussian fitting. For higher dose such as in the 500 Gy *vs.* 50 Gy irradiated difference spectrum, the band at 350 nm becomes predominant.

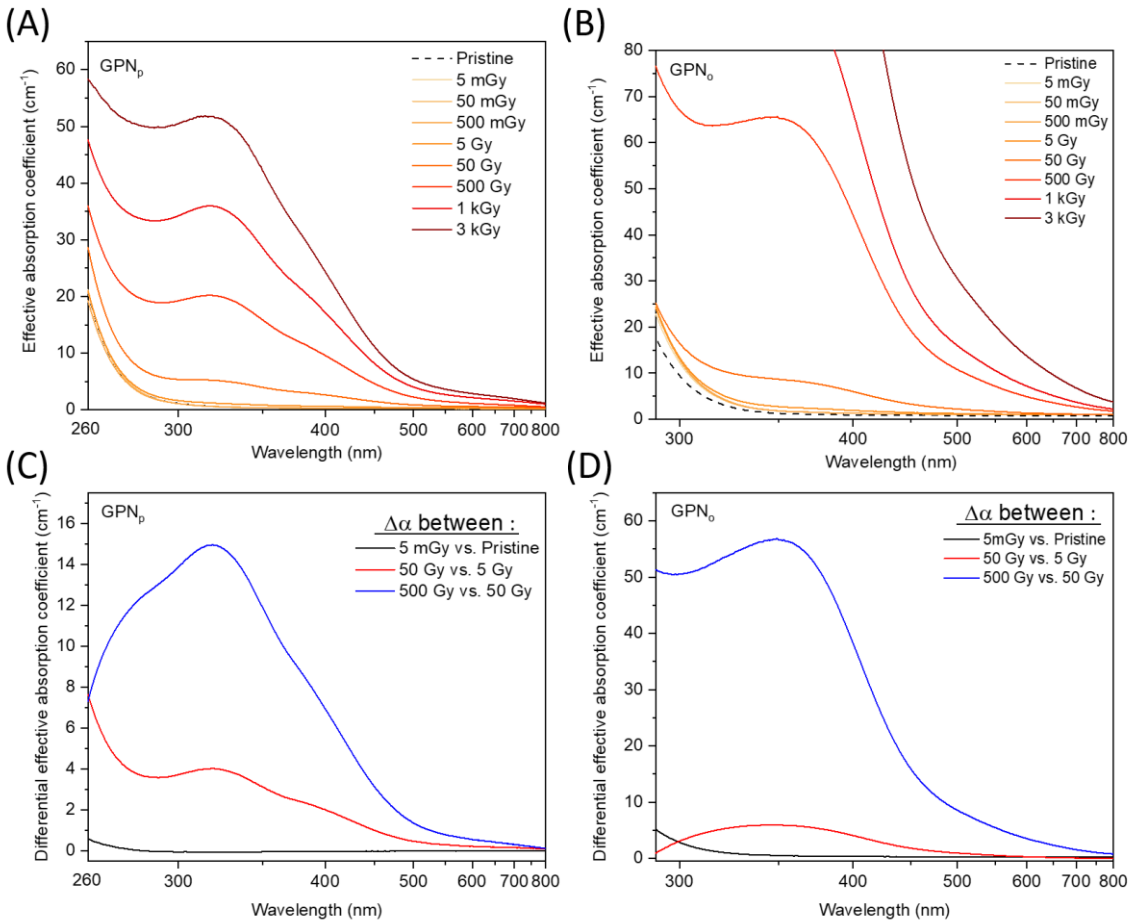

Figure 3 Radiation induced absorption spectra for GPN_p (A) and GPN_o (B) after various X-rays irradiation doses from 5 mGy to 3 kGy. The difference absorption coefficient spectra for 5 mGy vs. Pristine, 50 Gy vs. 5 Gy and 500 Gy vs. 50 Gy in both glass compositions is shown in (C) and (D), respectively.

The luminescence on each irradiated glass, for both glass compositions, has been performed at various excitation and emission wavelengths. The 650 nm and 500 nm excitation spectra, as well as the 320 nm emission spectra, are displayed in Figure 4 for both GPN glasses after a 500 Gy-dose irradiation. This specific dose has been selected in order to have a good compromise of the pristine and irradiated glass luminescence properties in both glass compositions. For an excitation at 320 nm (Figure 4C), the GPN_p glass exhibits a main emission band at 600 nm with a shoulder at about 500 nm, while for the same excitation, the GPN_o glass displays only one broad emission in the entire visible range centered at 520 nm. Considering the emission spectra at 650 nm (Figure 4A), the GPN_p glass shows the major excitation contribution bands at 270 nm, 320 nm and 370 nm. For 500 nm emission,

the excitation bands are located at about 240 nm and 355 nm. Meanwhile, for the GPN_o glass (Figure 4B), the red excitation spectrum highlights a broad band at 280 nm and a narrower one at 420 nm, while for the visible range excitation spectrum, the two latter bands are shifting at 290 nm and 390 nm respectively. The lifetime of the red and visible range emissions has been extracted from time-resolved spectroscopy experiments for GPN_p and GPN_o glasses under 355 nm excitation. In both glass compositions, the red emission centered at 600 nm is characterized by a 3 µs lifetime, while the visible range luminescence has a lifetime of about 5 ns.

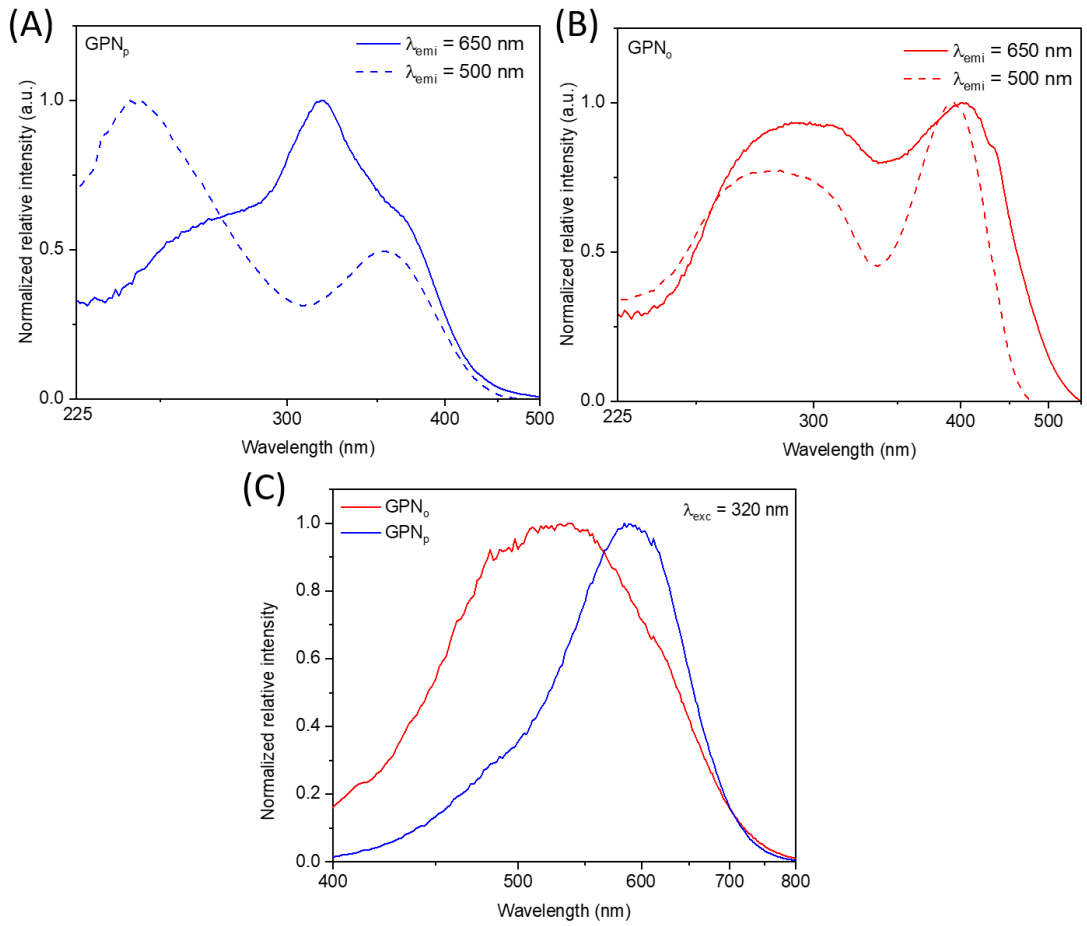

Figure 4 Luminescence of both GPN glass compositions after a 500 Gy-dose irradiation. Excitation spectra at 650 nm and 500 nm for GPN_o (A) and GPN_p (B) glasses. (C) Emission spectra for both glasses under an UV excitation at 320 nm.

Moreover, micro-luminescence measurements have been performed on the lateral edge of the glass, perpendicularly to the front X-rays irradiated face. Such lateral face had been optically polished before carrying out the luminescence experiment across the glass section. The emission

spectra were recorded, over a typical glass thickness of 1 mm, every 50 µm over a linear edge-to-edge cartography in both GPN glasses irradiated from 5 mGy to 5 kGy. Each cartography started few tens of microns prior to the glass edge, such initial lateral position corresponding to the 0 µm-depth. The evolution of the integrated spectral distribution in the entire spectrum at lateral position, corresponding to each depth of X-rays irradiation, is reported on Figure 5A (GPN_p) and 5D (GPN_o) for all X-rays doses. Figures 5B and 5E depict the spectral distribution evolution for a 500 Gy-dose at several depths while Figure 5C and 5F display it for a 50 µm-depth at several doses, for both GPN glasses. First, for the GPN_p glass, the integrated luminescence intensity increases with the dose. For the two highest doses, the intensity decrease does not drop as fast as for the other doses on first hundreds of micron. Meanwhile, at a given dose the intensity profile exhibits a general decrease, which naturally results from the X-rays attenuation during in-depth glass penetration (Figure 5A). As observed in Figure 5B, the spectral distribution is changing from the surface up to the deepest measured point. The nearest-from-the-surface recorded spectrum shows a wide band from 440 nm to 760 nm centered at about 520 nm. The deeper, the more red-shifted is the maximum intensity position. For the deepest spectrum, the maximal intensity peaks now at 620 nm. The spectral distribution evolution at a fixed depth of 50 µm has also been studied as depicted in Figure 5C. For the highest doses (1 and 5 kGy), the main contribution is centered at around 520 nm while for the lowest dose the weak luminescence spectrum peaks at around 620 nm. For the GPN_o glass, the integrated relative intensity evolution as function of the depth is presented on Figure 5D. Up to 50 Gy, the same intensity profile as in the GPN_p glass is observed. From 500 Gy to 5 kGy, the highest integrated intensity is no longer located near the front irradiated surface but rather moves towards the glass bulk. After this maximum, the integrated intensity declines with the depth. As observed on Figures 5E and 5F whether at fixed 500 Gy-dose or 50 µm-depth, the spectral distribution does not present any significant modifications.

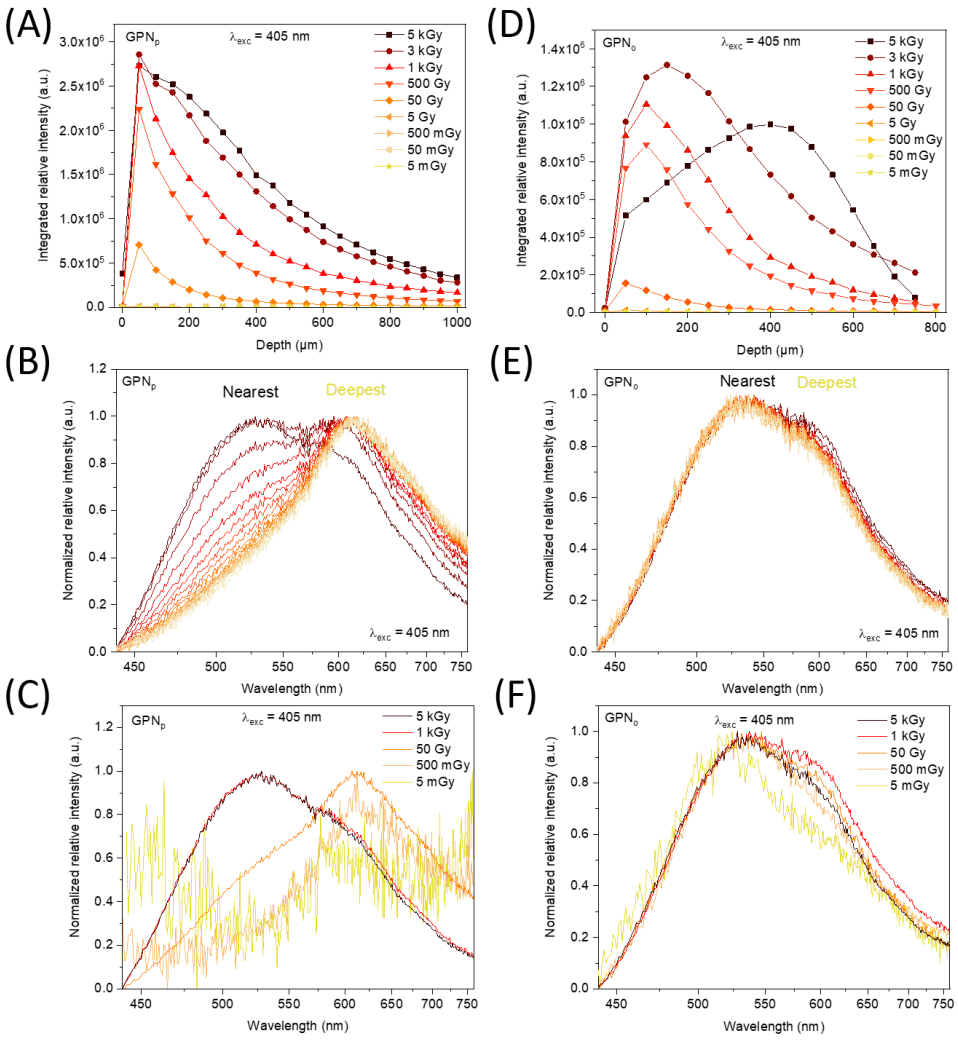

Figure 5 Micro-luminescence of irradiated GPN glasses performed on the glass optically polished side: (A),(D) integrated relative intensity, (B),(E) normalized spectrum evolution for the 500 Gy-dose and (C),(F) 50 µm-depth for the GPN_p and GPN_o glass compositions, respectively.

III-2. Investigation of the resilience to X-rays of IR fs DLW generated structures

A large 3×3 mm^2 square has been pre-inscribed by IR fs DLW at 160 µm below the GPN_p glass surface using an experimental procedure described elsewhere (12). Two different laser parameters were used in two identical GPN_p glass samples, corresponding to high and low DLW dose depositions (11). Both DLW depositions lead to a luminescence being dominated by the silver clusters Ag_m^{x+} (33) The respective laser parameters correspond to an irradiance of 13.4 $TW.cm^{-2}$ for a sample displacement velocity of 100 $\mu m.s^{-1}$ and an irradiance of 10 $TW.cm^{-2}$ for a sample displacement velocity

of 250 µm.s^{-1}. All-in-one radio-photo-luminescence (RPL) experiments (combining an X-rays irradiation and UV excitation at 355 nm) have been carried out on the fs laser inscribed samples. The RPL spectra were recorded every 10 seconds at a fixed dose rate of 0.2 Gy.s^{-1} for X-rays doses spanning from 2 Gy up to 188 Gy for the low DLW dose, and up to 376 Gy for the high DLW dose, as reported in Figure 6A and 6B respectively. Both samples present a wide band luminescence centered at 460 nm with a shoulder at around 620 nm. While increasing the X-rays dose, one observes that both samples act differently in terms of emission profiles. For the high DLW dose glass, the 460 nm-luminescence loses about half of its original intensity, while a 630 nm luminescence band appears and increases to become predominant beyond a dose of 112 Gy (Figure 6A). For the low DLW dose glass, the 630 nm luminescence band overcomes substantially the emission band at 460 nm after few tens of Gy (Figure 6B), while the 460 nm band remains stable all along the RPL experiment.

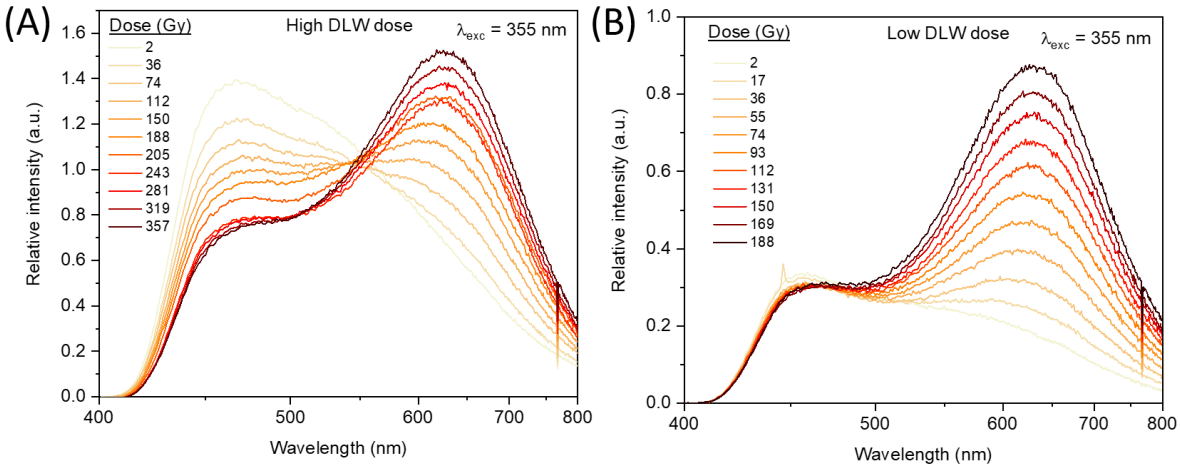

Figure 6 Radio-photo-luminescence measurement of the GPN$_p$ glass in which two square structures are generated by IR femtosecond direct laser writing at (A) high and (B) low laser dose.

To evaluate the effect of X-rays irradiation on the DLW luminescent structures, a micro-luminescence measurement under a laser diode excitation at 405 nm has been performed after the X-rays irradiation on a fresh optically polished glass edge in order to intersect the DLW structure, on both high and low dose laser written samples. The emission spectra were recorded every 2 µm during a linear cartography. The intensity profile of integrated spectral distribution for the higher DLW dose are presented hereafter on the Figure 7A. The positive continuous background displays a wide red band

centered at 630 nm, corresponding to the XR red curve on the Figure 7B. While approaching the femtosecond produced structures, the intensity profile increases sharply, with a corresponding 520 nm-luminescence (black curve – Figure 7B) characteristic of the Ag_m^{x+} silver clusters. The DLW structure luminescence before X-rays irradiation has been added in the Figure 7B in order to compare the spectral distribution, which corresponds to the DLW blue curve.

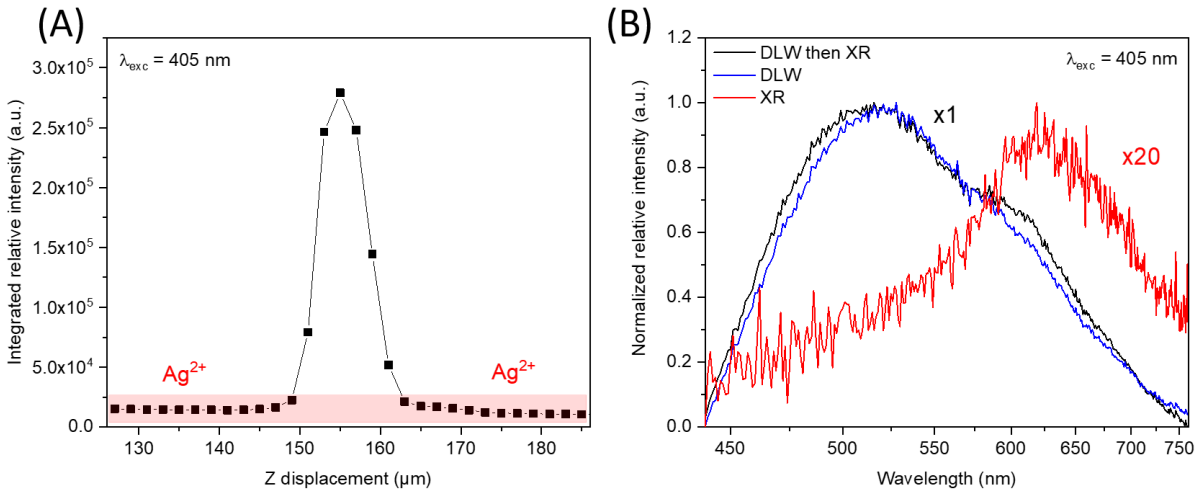

Figure 7 Linear micro-luminescence cartography under a 405 nm excitation of the GPN_p glass after a high DLW dose. (A) Intensity profile evolution over the glass depth. (B) Spectral distribution of the high DLW dose luminescence before RPL experiment corresponding respectively to blue and black curve. The red curve is related to the luminescence recorded outside of the DLW structure after X-Rays irradiation.

In Figure 8, the effective absorption coefficient has been measured and calculated for the GPN_p sample before any type of irradiation (dashed black curve), after the IR fs DLW inscription with Ag_m^{x+} (blue curve) and then irradiated during the RPL experiment up to a dose of about 400 Gy (red curve). Note that such effective absorption coefficient is estimated by taking into account the full thickness of the glass sample, while the highly absorbing silver clusters only spread over thickness of 5 to 10 µm. Amplitudes and profiles of the relative graphs in Figure 8B should be considered with caution. Indeed, the two resulting difference spectra between each experiment are depicted in the inset: respectively blue dashed curve corresponding to DLW structure *vs.* pristine glass and red dashed curve corresponding to X-rays exposure in the location of the DLW structure *vs.* DLW structure. In the DLW

structure *vs.* pristine glass differential absorption spectrum, two bands at 280 nm and 340 nm are noticeable. The DLW structure after and before X-rays irradiation differential spectrum shows an important band at 320 nm with an additional shoulder at 380 nm and tail below 300 nm.

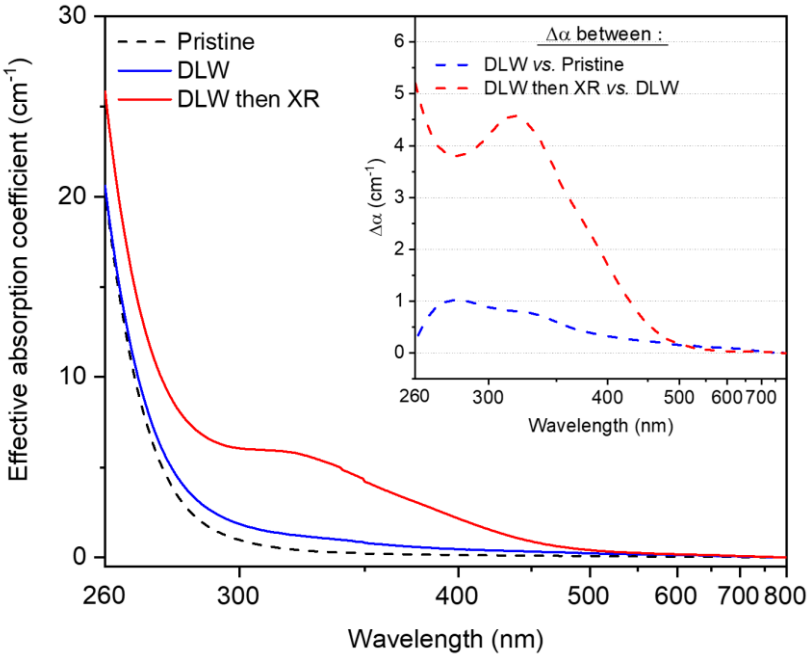

Figure 8 Effective absorption coefficient on pristine GPN_p glass, after high dose IR fs DLW and then irradiated by X-rays during RPL experiment. Inset shows the respective difference spectrum for DLW structure vs. *pristine glass and X-rays exposure in the location of the DLW structure* vs. *DLW structure.*

IV. Discussion

IV-1. Structural impact on X-rays irradiated phosphate photosensitivity

As described elsewhere (12), the increase of Na^+ sodium ion content in silver-doped GPN glasses leads to a progressive increase of the Oxygen-to-Phosphorus ratio, which is a good indicator of the glass structure (ultra-, poly-, pyro- or ortho-phosphate). However, acting as a network modifier, Na^+ sodium ions shrink the phosphate chains, which then decreases the glass durability. This aspect could be compensated by an increase of the Gallium content, since Masera *et al.* (34) have demonstrated an improvement of the glass chemical resistance in zinc-phosphate glass composition. The glass network

modification affects the glass properties such as density, refractive index, glass transition temperature, as reported in Table 1.

The Raman spectral response of the GPN_p, highlighting symmetrical stretching vibrations of P-O-P bonds and (PO_2^-) tetrahedron in Q^2 and Q^1 entities, indicates that GPN_p glass acts as a poly-phosphate and pyro-phosphate. However, with an O/P = 3.4 ratio closer to pyro-phosphate (O/P = 3.5) compared to poly-phosphate (O/P > 3), the GPN_p glass is considered as a pyro-phosphate. Meanwhile in the GPN_o glass, the absence of the P-O-P bonds spectral signature, as well as the presence of the (PO_4^3) symmetrical stretching vibrations, emphasizes an ortho-phosphate network behavior (O/P > 4) (23). Regarding the 640 cm^{-1} band contribution related to $[GaO_4]^-$ stretching vibration in both studied glasses, one observes a higher intensity in GPN_o glass than in the GPN_p. Indeed, previous observation could be explained by the intermediate role of the Gallium shifting from an octahedral site to a tetrahedral one when the Gallium-to-Phosphorous ratio is increasing (24,35), which is the case from GPN_p (Ga/P ratio = 0.5) to GPN_o (Ga/P ratio = 0.66) glasses. This phenomenon results in a covalent compensation of the depolymerized phosphate chains, which in turn strengthens the glass network (26,35).

The radioluminescence experiment in silver-doped phosphate glass is a powerful tool as it allows for following the emission evolution under X-rays irradiations. Tanaka *et al.* reported a luminescence study in many silver-doped phosphate glasses (36), and one of them containing Al_2O_3 allows for a reasonable comparison with GPN glasses. The silver luminescence (excitation and emission) decline is observed while increasing the X-rays dose, supported by either silver ion consumption, competitive absorption due to X-rays-generated species, or possibly both. Here, in Figure 2A, we report also a luminescence decrease with the X-rays dose, which is in good agreement with previous study from Tanaka *et al*. The RL experiment combining excitation and irradiation allows for a silver consumption tracking, as observed in Figure 2B. The RL spectral distribution being homothetic at various doses (Figure 2A - inset), the isolated silver ions Ag^+ (λ_{emi} = 290 nm) and silver pairings Ag^+-Ag^+ (λ_{emi} = 380 nm) are consumed at the same rate, no effect of re-absorption by the generation of new XR-induced silver-

based entities can be detected. This observation could be interpreted as isolated and paired silver ions act as a same silver reservoir, giving rise to the simplified X-rays irradiation process denoted as:

$$[Ag^{+}] + h\nu_{XRay} \rightarrow Ag^{2+} + Ag^{0}$$

The one-phase exponential decay mathematical expression of the silver reservoir [Ag^{+}] consumption. derives from the Beer-Lambert law (9) applied on Figure 2B is:

$$\frac{I_{(t)}}{I_{(0)}} = \exp(-r_c * t) + y_o \quad (1)$$

Where $I(t)$ is the dose-dependent transmitted intensity, $I_{(0)}$ is the initial relative intensity, r_c is the consumption rate, t the irradiation time and y_o is an offset. The determined consumption rates for both GPN_p and GPN_o glasses, assuming a limited effect of absorbing XR-produced species, are respectively of 0.0028 ±0.0002 s^{-1} and 0.0033 ±0.0002 s^{-1}. A 1st-order kinetic would indicate then that a constant proportion of the silver reservoir is consumed per unit of dose (or time).

As previously mentioned in the silver reservoir consumption, a one-phase exponential association mathematical expression derived from the Beer-Lambert law can be considered to model for the hole-trap center Ag^{2+} formation (Figure 5A) in GPN_p glasses in the case of high DLW dose:

$$I_{(t)} = Y_b + A(1 - \exp(-r_f * t)) \quad (2)$$

Where $I_{(t)}$ is the relative intensity, Y_b is a baseline, A is a coefficient function of the initial quantity of Ag^{2+} generating species, r_f is the Ag^{2+} formation rate and t is the irradiation time. From this equation (2), the formation rate r_f has been extracted and is set to 0.0033 ±0.0007 s^{-1}.

Considering the X-Rays irradiated GPN glasses in term of effective absorption coefficients (Figure 3A and 3B) and the GPN_p excitation/emission spectra (Figure 4), the main 620 nm emission band is related to the absorption/excitation bands peaking at 280 nm, 320 nm and 380 nm. The associated lifetime is around 3 µs and it corresponds to Ag^{2+} hole-trap silver species detected by EPR (not shown here) (5,6). In the GPN_p 500 Gy *vs.* 50 Gy differential absorption spectrum (Figure 3C), the band intensity ratio between contributions at 280 nm and 320 nm is noticeably different in comparison to the one in the 650 nm excitation spectrum. Such discrepancy may be related to the presence of additional absorption features. The wide 520 nm-emission with a lifetime below 10 ns is attributed to

Ag_m^{x+} silver clusters (14). The corresponding absorption range is from 280 nm to 500 nm. Finally, the formation of silver clusters is favored under X-rays irradiation in the GPN_o ortho-phosphate glass matrix, as compared to that of the GPN_p pyro-phosphate glass.

In the GPN_p glass, the spectral distribution evolutions with the dose or the depth (respectively Figure 5B and 5C) indicate that the Ag^{2+} hole-traps are first formed for the lowest doses, whereupon the silver clusters appear solely at a sufficient X-rays dose. Meanwhile in the GPN_o glass, the clusters are formed from the very first X-rays doses while a weak emission of Ag^{2+} is measured. As observed in Figure 5D, the intensity increasing feature in the first tens or hundreds of microns, depending of the X-rays dose, correlatively goes hand to hand with an increase of a competitive absorption phenomenon which could be related to the presence of non-luminescent electron traps such as Ag^0 (Figure 3B) (4,8).

IV-2. Investigation of the resilience to X-rays of IR fs DLW generated structures

At first glance, during the RPL process a significant increase of the Ag^{2+} luminescence overlays the DLW silver clusters luminescence. Nevertheless, there is no evidence of any partial destruction of the laser written silver clusters. Accordingly to Figure 8, for excitation at 355 nm, the decrease of the silver cluster emission at 460 nm (Figure 6A) seems to be related to a competitive absorption of exciton-trap species such as Ag^{2+} or Ag^0 (instead of a reduction of the silver cluster population).

The micro-luminescence experiment on the laser inscribed square structure in the GPN_p glass suggests then that the silver clusters luminescence survives to an X-rays irradiation of at least 357 Gy. This resilience is strongly supported by the conservation of the Ag_m^{x+} localization (Figure 7A) and emission spectral distribution (Figure 7B).

V. Conclusion

This work has investigated the structural impact of pyro- and ortho- silver-containing sodo-gallo-phosphate glasses subject to X-rays irradiations. The shortening of phosphate tetrahedra connectivity influences the nature of the silver ionic species initially present in the glass, resulting in the increase of silver pairing at the expense of the isolated silver ions. Moreover, the subsequent silver species

generated by X-rays irradiation, namely Ag^{2+} hole trap silver ions and Ag_m^{x+} silver clusters, are clearly identified and point out an improved ability of the silver ions to capture the electron and hole in the ortho-phosphate glass. Second part of this study has been focused on the subsistence of the fs laser written structures, which has been validated for the first time for X-rays irradiation up to a 357 Gy-dose.

Acknowledgement and support

The authors acknowledge Angelo Monguzzi for providing the 355 nm Nd:YAG laser allowing the real time RPL measurement. This work has been carried out in the frame of the EIT SPARK Project (16290), by the French National Research Agency (ANR-17-CE08-0042-01), “the investments for the future” Programme IdEx Bordeaux – LAPHIA (ANR-10-IDEX-03-02) and the Region “Nouvelle Aquitaine” in the frame of the FabMat project (2016-1R10107).

Reference

1. Schulman JH, Shurcliff W, Ginther RJ, Atti FH. Radiophotoluminescence dosimetry system of the U.S. NAVY. Nucleonics Ceased publication. 1953;11(10).
2. Piesch E, Burgkhardt B. Photoluminescence dosimetry : the alternative in personnel monitoring. Radioprotection. janv 1994;29(1):39-67.
3. Becker K. Some characteristics of RP L dosimeter glasses. 1967.
4. McKeever SWS, Sholom S, Shrestha N. Observations regarding the build-up effect in radiophotoluminescence of silver-doped phosphate glasses. Radiation Measurements. avr 2019;123:13-20.
5. Bourhis K, Royon A, Papon G, Bellec M, Petit Y, Canioni L, et al. Formation and thermo-assisted stabilization of luminescent silver clusters in photosensitive glasses. Materials Research Bulletin. avr 2013;48(4):1637-44.
6. Hsu SM, Yung SW, Brow RK, Hsu WL, Lu CC, Wu FB, et al. Effect of silver concentration on the silver-activated phosphate glass. Materials Chemistry and Physics. sept 2010;123(1):172-6.
7. Dmitryuk AV, Paramzina SE, Perminov AS, Solov’Eva ND, Timofeev NT. The influence of glass composition on the properties of silver-doped

radiophotoluminescent phosphate glasses. Journal of non-crystalline solids. 1996;202(1-2):173–177.
8. Miyamoto Y, Takei Y, Nanto H, Kurobori T, Konnai A, Yanagida T, et al. Radiophotoluminescence from silver-doped phosphate glass. Radiation Measurements. déc 2011;46(12):1480-3.
9. Syutkin VM, Dmitryuk AV, Tolkachev VA. Kinetics of formation of di- and trinuclear silver complexes in radiophotoluminescent glasses. Fizika i Khimiya Stekla. 1992;18(3):66-76.
10. Ershov BG, Ionova GV, Kiseleva AA. Silver clusters: calculations of optical transitions and the formation and properties of « magic » positively charges clusters. Russian Journal of Physical Chemistry. 1995;689(2):239-48.
11. Petit Y, Danto S, Guérineau T, Abou Khalil A, Le Camus A, Fargin E, et al. On the femtosecond laser-induced photochemistry in silver-containing oxide glasses: mechanisms, related optical and physico-chemical properties, and technological applications. Advanced Optical Technologies. 25 oct 2018;7(5):291-309.
12. Guérineau T, Loi L, Petit Y, Danto S, Fargues A, Canioni L, et al. Structural influence on the femtosecond laser ability to create fluorescent patterns in silver-containing sodium-gallium phosphate glasses. Optical Materials Express. 1 déc 2018;8(12):3748.
13. Royon A, Bourhis K, Bellec M, Papon G, Bousquet B, Deshayes Y, et al. Silver Clusters Embedded in Glass as a Perennial High Capacity Optical Recording Medium. Advanced Materials. 7 déc 2010;22(46):5282-6.
14. Bellec M, Royon A, Bourhis K, Choi J, Bousquet B, Treguer M, et al. 3D Patterning at the Nanoscale of Fluorescent Emitters in Glass. The Journal of Physical Chemistry C. 23 sept 2010;114(37):15584-8.
15. Papon G, Petit Y, Marquestaut N, Royon A, Dussauze M, Rodriguez V, et al. Fluorescence and second-harmonic generation correlative microscopy to probe space charge separation and silver cluster stabilization during direct laser writing in a tailored silver-containing glass. Optical Materials Express. 1 nov 2013;3(11):1855.
16. Papon G, Marquestaut N, Petit Y, Royon A, Dussauze M, Rodriguez V, et al. Femtosecond single-beam direct laser poling of stable and efficient second-order nonlinear optical properties in glass. Journal of Applied Physics. 21 mars 2014;115(11):113103.
17. Canioni L, Bellec M, Royon A, Bousquet B, Cardinal T. Three-dimensional optical data storage using third-harmonic generation in silver zinc phosphate glass. Optics letters. 2008;33(4):360–362.
18. Shakhgildyan GYu, Lipatiev AS, Vetchinnikov MP, Popova VV, Lotarev SV, Golubev NV, et al. One-step micro-modification of optical properties in silver-doped zinc phosphate glasses by femtosecond direct laser writing. Journal of Non-Crystalline Solids. févr 2018;481:634-42.

19. Marquestaut N, Petit Y, Royon A, Mounaix P, Cardinal T, Canioni L. Three-Dimensional Silver Nanoparticle Formation Using Femtosecond Laser Irradiation in Phosphate Glasses: Analogy with Photography. Advanced Functional Materials. oct 2014;24(37):5824-32.
20. Abou Khalil A, Bérubé J-P, Danto S, Desmoulin J-C, Cardinal T, Petit Y, et al. Direct laser writing of a new type of waveguides in silver containing glasses. Scientific Reports [Internet]. déc 2017 [cité 19 sept 2017];7(1). Disponible sur: http://www.nature.com/articles/s41598-017-11550-0
21. Abou Khalil A, Bérubé J-P, Danto S, Cardinal T, Petit Y, Canioni L, et al. Comparative study between the standard type I and the type A femtosecond laser induced refractive index change in silver containing glasses. Optical Materials Express. 1 juin 2019;9(6):2640.
22. Brow RK. Review: the structure of simple phosphate glasses. Journal of Non-Crystalline Solids. mars 2000;263-264:1-28.
23. Brow RK. Nature of Alumina in Phosphate Glass: I, Properties of Sodium Aluminophosphate Glass. Journal of the American Ceramic Society. avr 1993;76(4):913-8.
24. Hee P, Christensen R, Ledemi Y, Wren JEC, Dussauze M, Cardinal T, et al. Properties and structural investigation of gallophosphate glasses by 71Ga and 31P nuclear magnetic resonance and vibrational spectroscopies. J Mater Chem C. 2014;2(37):7906-17.
25. Belkébir A, Rocha J, Esculcas AP, Berthet P, Poisson S, Gilbert B, et al. Structural characterization of glassy phases in the system Na2O–Ga2O3–P2O5 by MAS-NMR, EXAFS and vibrational spectroscopy. I. Cations coordination. Spectrochimica Acta Part A: Molecular and Biomolecular Spectroscopy. févr 2000;56(3):423-34.
26. Belkébir A, Rocha J, Esculcas AP, Berthet P, Gilbert B, Gabelica Z, et al. Structural characterization of glassy phases in the system Na2O–Ga2O3–P2O5 by MAS and solution NMR and vibrational spectroscopy: II. Structure of the phosphate network. Spectrochimica Acta Part A: Molecular and Biomolecular Spectroscopy. févr 2000;56(3):435-46.
27. Ilieva D, Jivov B, Bogachev G, Petkov C, Penkov I, Dimitriev Y. Infrared and Raman spectra of Ga2O3–P2O5 glasses. Journal of Non-Crystalline Solids. mai 2001;283(1-3):195-202.
28. Velli LL, Varsamis CPE, Kamitsos EI, Möncke D, Ehrt D. Structural investigation of metaphosphate glasses. 2005;46(2):4.
29. Fukunaga J, Bando R, Ota R, Yoshida N. Raman Spectra and Structure of Glasses in the System Na2O-Ga2O3-B2O3. Journal of the Ceramic Society of Japan. 1988;96(1114):634-8.
30. Zhao Y, Frost RL. Raman spectroscopy and characterisation of α-gallium oxyhydroxide and β-gallium oxide nanorods. Journal of Raman Spectroscopy. oct 2008;39(10):1494-501.

31. Dohy D, Lucazeau G. Raman Spectra and Valence Force Field of Single-Crystalline β Ga2O3. 1982;45(2):180-92.
32. Belharouak I, Parent C, Gravereau P, Chaminade JP, Le Flem G, Moine B. Luminescent Properties of Silver(I) Diphosphate of Compositions Na2−xAgxZnP2O7. Journal of Solid State Chemistry. févr 2000;149(2):284-91.
33. Bourhis K, Royon A, Bellec M, Choi J, Fargues A, Treguer M, et al. Femtosecond laser structuring and optical properties of a silver and zinc phosphate glass. Journal of Non-Crystalline Solids. oct 2010;356(44-49):2658-65.
34. Massera J, Bourhis K, Petit L, Couzi M, Hupa L, Hupa M, et al. Effect of the glass composition on the chemical durability of zinc-phosphate-based glasses in aqueous solutions. Journal of Physics and Chemistry of Solids. janv 2013;74(1):121-7.
35. Ren J, Eckert H. Intermediate Role of Gallium in Oxidic Glasses: Solid State NMR Structural Studies of the Ga2O3–NaPO3 System. The Journal of Physical Chemistry C. 17 juill 2014;118(28):15386-403.
36. Tanaka H, Fujimoto Y, Saeki K, Koshimizu M, Yanagida T, Asai K. Radiophotoluminescence properties of Ag-doped mixed phosphate glasses. Radiation Measurements. nov 2017;106:180-6.
37. Fan S, Yu C, He D, Li K, Hu L. Gamma rays induced defect centers in phosphate glass for radio-photoluminescence dosimeter. Radiation Measurements. janv 2011;46(1):46-50.